Lagrangian analysis of fluid transport in empirical vortex ring flows

Shawn C. Shadden
Control and Dynamical Systems, California Institute of Technology, Pasadena, California 91125

John O. Dabiri
Graduate Aeronautical Laboratories and Bioengineering, California Institute of Technology, Pasadena, California 91125

Jerrold E. Marsden
Control and Dynamical Systems, California Institute of Technology, Pasadena, California 91125

(Received 23 January 2006; accepted 3 March 2006; published online 17 April 2006)

In this paper we apply dynamical systems analyses and computational tools to fluid transport in empirically measured vortex ring flows. Measurements of quasisteadily propagating vortex rings generated by a mechanical piston-cylinder apparatus reveal lobe dynamics during entrainment and detrainment that are consistent with previous theoretical and numerical studies. In addition, the vortex ring wake of a free-swimming *Aurelia aurita* jellyfish is measured and analyzed in the framework of dynamical systems to elucidate similar lobe dynamics in a naturally occurring biological flow. For the mechanically generated rings, a comparison of the net entrainment rate based on the present methods with a previous Eulerian analysis shows good correspondence. However, the current Lagrangian framework is more effective than previous analyses in capturing the transport geometry, especially when the flow becomes more unsteady, as in the case of the free-swimming jellyfish. Extensions of these results to more complex flow geometries is suggested. © *2006 American Institute of Physics*. [DOI: 10.1063/1.2189885]

I. INTRODUCTION

A. Overview

The kinematic flow structure of two empirically measured, unsteady vortex flows is studied using dynamical systems analyses. In particular, entrainment and detrainment of fluid is examined. The first flow considered is that of a propagating vortex ring and the second is that of the flow surrounding a free-swimming *Aurelia aurita* jellyfish. As we explain in more detail later, examples like the jellyfish show that there is a need to extend previous tools, which relied on the use of lobe dynamics that are revealed in Poincaré sections in periodic or near periodic Eulerian velocity fields, to a fully unsteady context. Our purpose in this paper is to carry out this extension by showing that the computation of Lagrangian coherent structures (LCS) reveals time-dependent structures in the fully unsteady case, which play the role of heteroclinic lobe structures in the periodic case.

B. History of lobe dynamics associated to vortex rings

The study of vortex rings has a long history and is reviewed in the paper by Shariff and Leonard.[1] Particularly noteworthy in that work, and in Refs. 2 and 3, is the characterization of entrainment and detrainment through lobe dynamics, which is reviewed in Sec. II A. Motivated by the work of Leonard, Rom-Kedar, and Wiggins,[4] Shariff and coworkers show, using theoretical and numerical analyses, the occurrence of heteroclinic tangles of the stable and unstable manifolds of the front and rear stagnation points in a Poincaré section of a model vortex ring.[5] The Poincaré section was constructed from the periodic motion produced by the vortex model's characteristic frequency, which corresponded to the rotation of its elliptical core. The evolution of the associated manifolds into lobes was shown to govern the entrainment and detrainment of fluid from the vortex ring. In addition, the computed flow geometry agreed qualitatively with smoke[6] and schlieren[7] visualizations, as well as previous theoretical and numerical observations of spike formation behind vortex rings.[8,9]

Rom-Kedar and co-workers[10,11] offered a more refined understanding of the role of lobe formation in the entrainment/detrainment processes. The analytic oscillating vortex pair studied in Ref. 11 was given by a stream function of the form

$$\Phi(x,y,t) = \Phi_0(x,y) + \epsilon\Phi_1(x,y,t),$$

where $\Phi_0(x,y)$ defines the steady flow of counter-rotating point vortices and $\Phi_1(x,y,t)$ is a time-periodic perturbation scaled by the strain rate amplitude, ϵ. Rom-Kedar *et al.*, proved the existence of lobe dynamics (and the associated horseshoe map), and also developed estimates of the flux rate into and out of the vortex neighborhood, and performed a detailed study of residence times of particles in, or near, the vortex pair. Krasny and Nitsche[12] went beyond the case of a strictly periodic velocity field and used point-vortex simulations to show that for vortex pairs that exhibit a well-defined fundamental oscillation frequency, this frequency can be used to construct Poincaré sections, which display the generic chaotic features, including the heteroclinic tangle geometry, found in the works of Shariff *et al.* and Rom-Kedar *et al.* The work of Carnevale and Kloosterziel[13] demon-

strated lobe shedding from dye visualizations of vortices produced from rotating tank experiments and attributed these lobes to the same dynamical processes studied by Rom-Kedar *et al.*,[11] and made qualitative comparisons of the visualizations with their own numerical simulations.

C. Treating fully aperiodic flows

What separates the work presented here on vortex ring entrainment and detrainment from these past studies is the ability to compute the explicit geometry of the time-dependent structures that correspond to heteroclinic tangles in the periodic case, from empirical data of aperiodic vortex propagation.

The second flow considered in this paper is that surrounding a live, free-swimming *Aurelia aurita* jellyfish. Although previous qualitative studies have indicated that these animals form vortex rings during their swimming and feeding behaviors,[14] there were no quantitative measurements of the associated flow velocity field available up until now. Using quantitative visualization techniques such as digital particle image velocimetry (DPIV[15,16]), it is now possible to obtain detailed measurements of the velocity field of such complex fluid flows.

While there is an obvious (approximate) periodicity associated with the usual motion of the jellyfish itself, there is no clear periodic structure in the Eulerian velocity field of the fluid surrounding the animal. While propagating vortex rings have, arguably, an approximate periodicity in their Eulerian velocity fields due to departures from the steady Hill or Norbury family of vortices (see Sec. II A for a further discussion), that does not seem to be the case with jellyfish flows. In addition, the flow is not a small perturbation of an analytically known vortex flow, so perturbation methods do not appear to be the right tool for these types of problems. Of course jellyfish and other flows (for example, some cardiovascular flows[17] and microfluidic flows as well[18,19]) are even more complex as the animal undergoes turning and accelerating maneuvers and we wish to have a tool capable of analyzing such situations as well.

As we have indicated, the theoretical and numerical studies mentioned previously have been facilitated by time periodicity (or aperiodicity with a dominant frequency[12]); empirical vortex ring flows such as those in naturally occurring biological systems will often be fully aperiodic. Another complication is that in such fully aperiodic cases, there are not always obvious equilibrium points (or other invariant structures) on which to "hang" the invariant manifolds. Hence, in these cases it is not obvious whether lobe dynamics—if they occur at all—will manifest themselves in the same manner as in the aforementioned theoretical and numerical studies. A resolution to this question is an important step toward improving our understanding of biological fluid transport, thereby enabling therapies for malfunction (e.g., cardiovascular flows[20]) and the realization of bio-inspired engineering designs (e.g., bio-inspired transportation systems).

D. Objective of the paper

The objective is to apply methods of quantitative visualization, especially DPIV, to analyze empirical vortex ring flows in a Lagrangian dynamical systems framework. Using the concept of *Lagrangian coherent structures* (LCS[21–25]), the measured flows are examined to deduce lobe dynamics and their effect on entrainment and detrainment. Both a mechanical piston-cylinder vortex ring generator and live, free-swimming *Aurelia aurita* jellyfish are examined to compare the results of quasiperiodic flows previously examined to more complex biological flows of practical importance.

Although previous empirical studies have combined quantitative imaging and concepts from dynamical systems to analyze Lagrangian fluid transport,[26–28] the goal here is to examine the specific phenomena of lobe formation and fluid transport in empirical vortex ring flows. The coherent vortex ring structures examined here are important both for their ubiquitous occurrence in biological flows and for the fact that, as declared by Saffman,[29] the vortex ring "exemplifies the whole range of problems of vortex motion."

E. Outline

In Sec. II we review the role of lobe dynamics in the entrainment/detrainment of fluid to/from vortex rings and the methods used to extract this geometry from the empirical data. Section III describes the experimental methods used to measure the vortex ring flows generated by the mechanical piston-cylinder apparatus and the free-swimming jellyfish. In Sec. IV we present an analysis of the empirical vortex ring flows. In that section, a quantitative comparison is made with an Eulerian analysis of isolated vortex rings.[30] We conclude the paper in Sec. V with a discussion of the possible extensions of these results to more complex flows in nature and technology.

II. ANALYTICAL METHODS

A. Lobe dynamics

In this section we review, for the reader's convenience, lobe dynamics and its role in entrainment and detrainment in vortex rings; for more information about the fundamental theory; see Refs. 2 and 11. Henceforth, the transport of fluid particles is given a kinematic description, which can be summarized by the ordinary differential equation,

$$\dot{\mathbf{x}}(t) = \mathbf{v}[\mathbf{x}(t), t],$$

where $\mathbf{v}(\mathbf{x},t)$ denotes the Eulerian velocity field of the fluid, $\mathbf{x}(t)$ denotes the trajectory of a fluid particle, and t denotes time. For the current studies, $\mathbf{v}[\mathbf{x}(\mathbf{t}),\mathbf{t}]$ is obtained from DPIV, as described in Sec. III.

Figure 1 shows streamlines of Hill's spherical vortex.[31] The velocity field is time independent so that these streamlines represent fluid trajectories. Point A denotes the (hyperbolic) stagnation point in what we will consider the front of the vortex and point B denotes the (hyperbolic) stagnation point on the rear of the vortex. The stable manifolds of point B are the trajectories that asymptote to point B in forward

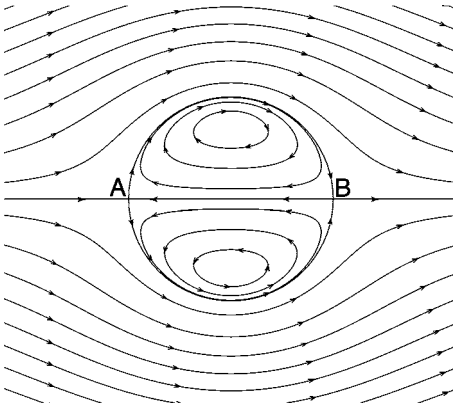

FIG. 1. Streamlines of Hill's spherical vortex.

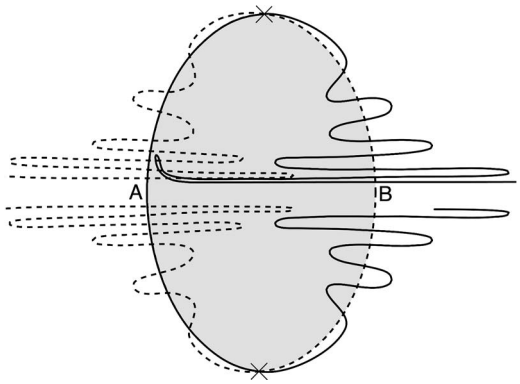

FIG. 3. Cartoon of heteroclinic intersections for a perturbed elliptical vortex. The interior of the vortex is given by the shaded region.

time and, in this case, coincide with the unstable manifolds of stagnation point A, i.e., the trajectories that asymptote to A as $t \to -\infty$. Such *heteroclinic* trajectories, which connect two stagnation points, are often called *separatrices* because they separate dynamically distinct regions in the flow. The vortex ring exemplifies this standard paradigm since these trajectories separate the circulating fluid from the irrotational flow that passes around the ring. Therefore, it is reasonable to define the boundary of the vortex ring as the union of these trajectories and the associated stagnation points.

It is well known that heteroclinic connections in time-independent systems are typically broken by the introduction of time-periodic perturbations.[1–3,10,11,32,33] For such systems the velocity field **v** is time dependent, albeit periodic. Typically, time-periodic systems are viewed as time-independent systems by looking at the evolution at fixed intervals of time, equal to the period of **v**; that is, via a *Poincaré section*. The stagnation points A and B in the unperturbed system typically remain fixed points (perhaps slightly perturbed in position) in the Poincaré section. However, the heteroclinic connection will often break and transversely intersect (in fact, in this special case one can prove that the manifolds are infinitely long and an infinite number of transverse intersections occur).

Such behavior is illustrated in Fig. 2 (see also Refs. 2, 3, 10, and 11). The unstable manifold of point A is depicted by the solid line and the stable manifold of point B is depicted by the dashed line. Notice that each manifold loops progressively back and forth as it approaches the other fixed point. To keep the illustration from becoming convoluted, only part of each manifold is shown in Fig. 2. The intersection of these manifolds creates regions called *lobes*. Each manifold is *invariant*, meaning that fluid particles do not cross these curves, or in fluid mechanics terminology, they are *material curves*. Therefore the lobes trap fluid that is confined to remain in the lobe as time evolves. The motion of these lobes can be quite predictable, which can help elucidate the transport and mixing processes.

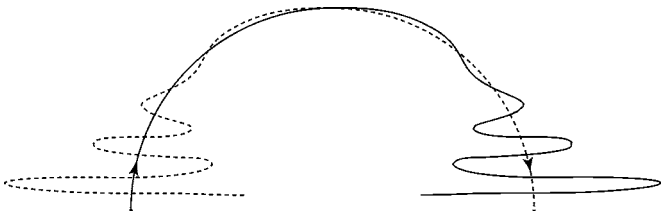

FIG. 2. Cartoon of the heteroclinic tangle of the upper unstable and stable manifolds of the front and rear stagnation points.

Vortex ring generation in a real fluid typically results in more oblate structures than Hill's spherical vortex (see Ref. 34 for an exception). In general, the shape of the vortex ring will depend on the distribution of vorticity that is delivered by the vortex generator. Although this distribution is usually not linear with radial position, as in Hill's spherical vortex, and the Norbury vortex family more broadly,[35] the flow topology in real vortex rings is similar. Therefore, in empirical flows, we might expect the appearance of patterns similar to those observed in previous theoretical and numerical studies,[2,3,8–12] as depicted in Fig. 3. Again the unstable manifolds are given by the solid lines while the stable manifolds are depicted by the dashed lines.

To understand how fluid is transported into and out of the vortex ring, we must first define the vortex interior. There are natural intersection points of the stable and unstable manifolds that can be used.[2,3,11] An X has been placed over these intersection points in Fig. 3. The interior of the vortex is then given by the intersection of the volumes enclosed by the unstable and stable manifolds, which is shown by the shaded region of Fig. 3. Since the stable and unstable manifolds given in Fig. 3 are invariant, particles on one side of a manifold must remain on that side when advected. The fluid in the interior of the shaded region is the recirculating flow. However, since there is entrainment and detrainment we know that some fluid outside the vortex will end up in the interior and *vice versa*; we next review how this occurs.

Lobe A, in Fig. 4(a), is nominally outside the vortex (if one likes, the lobe below A can be taken, and so on). As shown by Shariff *et al.*,[2,3] if we advect this lobe by the flow, it will continuously deform into a lobe similar to lobe B (or gets mapped to lobe B by the Poincaré map). Further evolution by the flow will continue to deform this lobe into lobes analogous to C, D, and then E. We have thus taken a lobe that is initially located outside the vortex and shown how it is advected, or entrained, inside of the vortex. To summarize, *it is the deformation of these manifolds over time, which*

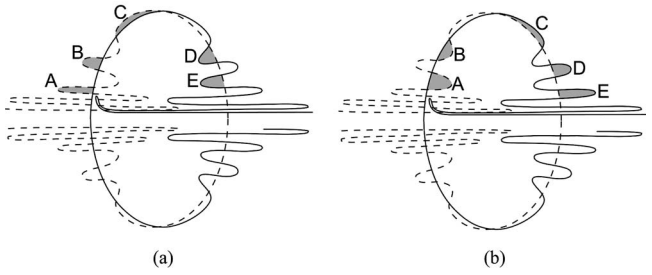

FIG. 4. Panel (a) illustrates the process of vortex ring fluid entrainment; panel (b) illustrates the process of fluid detrainment from the vortex ring.

causes the entrainment, not fluid crossing these manifolds.

Similarly, Fig. 4(b) shows how the detrainment of fluid from lobes initially inside the vortex to lobes outside the vortex can occur. Lobe A continually deforms into a lobe analogous to lobe E as time evolves. As time progresses, the lobes become narrower and longer, and for the case of the detrained lobes, they form thin filaments behind the vortex. As mentioned previously, these detrained spikes have been noticed in a variety of previous works.[2,3,8,9,11–13]

Neither stable nor unstable manifolds can self-intersect. Consistent with this impossibility of self-intersections, the lobes within the vortex will begin to wrap (fold) around the interior of the vortex, as shown by the thin lobe formed from the unstable manifold in Figs. 3 and 4. As these lobes become thinner and longer, they spiral farther into the interior of the vortex. A parcel of particles on either side of the stable manifold will be stretched apart as it approaches the rear, hyperbolic point B and it will also align with the long loops or filaments formed by the unstable manifold. This stretching and folding of fluid parcels is the distinguishing trait of chaotic mixing.[36] From these figures it should also be apparent that these entrained lobes will eventually intersect lobes that are detrained. Such *secondary intersections* explain how fluid that was once entrained can be later detrained from the vortex; see Ref. 11 for a further discussion.

Although the existence of the manifolds shown in Figs. 3 and 4 has been proven for near-integrable or quasiperiodic model vortex rings, and given as an explanation for the lobe shedding seen in dye visualizations of experimentally produced flows, analytic techniques have not previously been used to obtain the detailed lobe dynamics structure in empirical vortex ring flows. Such an analysis is important, for example, to be able to quantify transport rates, especially for engineering or biological applications. Relying on techniques for locating hyperbolic manifolds in aperiodic systems, we compute below the exact lobe dynamics structure in the vortex ring flows created by a mechanical vortex generator and free-swimming jellyfish. In the next section we overview the use of finite-time Lyapunov exponent (FTLE) fields for locating these structures.

B. Lagrangian coherent structures

In a series of papers,[21–24,37,38] Haller and co-workers give refined versions of necessary and sufficient conditions for the existence of "finite-time hyperbolic manifolds" in aperiodic flows, which are analogous to the traditional invariant manifolds that are defined[32] for time-independent, or time-periodic, systems. These "finite-time hyperbolic manifolds" are referred to as *Lagrangian coherent structures* (LCS). Those papers also point out the strong correspondence between the LCS defined from Haller's criteria and LCS obtained from finite-time Lyapunov exponent (FTLE) fields. In particular, Haller[24] notes that the FTLE fields admit ridges along the locally strongest hyperbolic lines, a notion that is studied further in Ref. 25. While other methods exist for locating hyperbolic trajectories in aperiodic velocity fields, our experience is that FTLE fields offer a particularly practical and robust method that is relatively straightforward to implement. The papers of Wiggins[39] and Jones and Winkler[40] review some other existing methods that have been developed to locate finite-time hyperbolic structures, and their application to flows representative of those found in geophysical fluid dynamics. See also Refs. 41 and 42 for other interesting studies of related phenomena in geophysical flows.

Finite-time Lyapunov exponent fields

The FTLE field measures, near a given point and at a given time, the maximum exponential divergence of nearby trajectories over a finite time-interval. Since the FTLE is derived from fluid trajectories, it is thought of as a Lagrangian quantity (although its advection properties are not obvious[25]). FTLE fields offer a convenient way to reveal transport barriers in the flow, even for systems with general time dependence and that are perhaps defined only over a finite interval of time.[22,24,25,43–46] Finite-time analysis is important in the study of both numerically and empirically generated datasets of aperiodic flows, such as those acquired during the analysis of engineering or biological fluid transport systems. Furthermore, the FTLE is independent of the reference frame.

Let $\phi_t^{t+T}:\mathbf{x}(t)\mapsto\mathbf{x}(t+T)$ denote the flow map, which maps fluid particles from their initial location at time t to their location at time $t+T$. The FTLE is given by

$$\sigma_t^T(\mathbf{x}) = \frac{1}{|T|}\ln\left\|\frac{d\phi_t^{t+T}(\mathbf{x})}{d\mathbf{x}}\right\|, \tag{1}$$

and measures the linearized (maximum) exponential growth rate over the interval T of trajectories starting near point $\mathbf{x}$ at time t. In (1), the norm is tacitly taken to be the induced L_2 norm, the "spectral norm." Additionally, $|T|$ is used instead of T because computing the FTLE for $T>0$ and $T<0$ produces LCS akin to stable and unstable manifolds, respectively, and thus the definition facilitates forward and backward time computations. For instance, two points straddling a stable manifold of a hyperbolic point typically separate much faster than other arbitrary particle pairs due to the exponential divergence they experience as they approach the hyperbolic point.[47] Likewise, two points straddling an unstable manifold will similarly have more pronounced separation than other pairs of points when advected backward in time. This is (heuristically) why ridges of high FTLE correspond to stable/unstable manifolds in autonomous or periodic sys-

tems, or more generally attracting LCS and repelling LCS in aperiodic flows.

The integration length $|T|$ is chosen according to the particular flow being analyzed. In general, longer integration times help reveal more of the LCS, such that as the integration time increases, the LCS grows in length. However practical issues typically bound the size of $|T|$ that can be considered, such as the temporal length or spatial domain limits of the numerically or empirically generated dataset.[25] The use of FTLE fields to locate LCS will become clearer in Sec. IV, which presents the results. In the next section we address the experimental methods used to obtain the velocity fields of the mechanically generated vortex rings and the flow about the *Aurelia aurita* jellyfish.

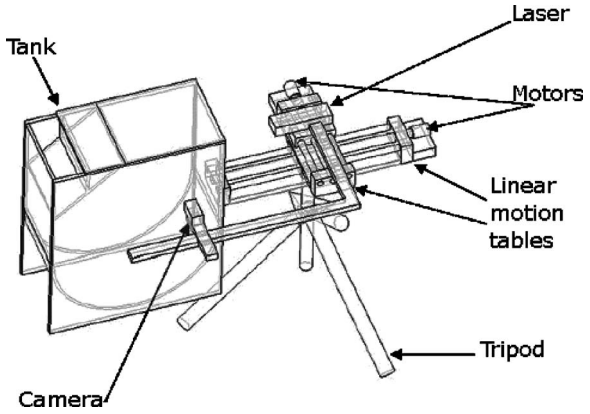

FIG. 5. Water tank and imaging apparatus for quantitative studies of jellyfish swimming and feeding.

III. EXPERIMENTAL METHODS

A. Mechanically generated vortex rings

Vortex rings were generated in the laboratory from the methods described in Dabiri and Gharib.[30] A piston-cylinder apparatus was submerged in a water tank and driven by a constant-head flow source ($\Delta p = 8.2$ kPa). The device created vortex rings by impulsively ejecting a jet of fluid with length-to-diameter ratio $L/D=2$ into the surrounding quiescent fluid. All of the fluid ejected during the vortex formation process created a single vortex ring, since the fluid jet length-to-diameter ratio was kept well below $L/D=4$, the dimensionless time after which vortex ring pinch-off ensues.[48] After the formation process, the vortex ring subsequently propagated downstream under its self-induced velocity.

Flow fields created by the piston-cylinder apparatus were measured by DPIV. A meridian symmetry plane of the axisymmetric flow was illuminated by a pulsed Nd:YAG laser sheet. Glass spheres (13 micron nominal diameter) seeded in the flow reflected incident laser light onto a digital (CCD) camera oriented with its image plane parallel to the laser sheet. Particle image patterns from adjacent camera frames were interrogated by the method of Willert and Gharib[16] to determine the corresponding velocity field. Vorticity fields were subsequently computed based on the measured velocity fields. Velocity and vorticity measurements possess an uncertainty of 1% and 3%, respectively.

The physical dimensions of the vortex generator (i.e., exit diameter $D_e = 2.54$ cm, exit velocity $U_e = 5.5$ cm s^{-1}) lead to a nominal flow Reynolds number of approximately 1400. The Reynolds number calculated based on the vortex ring circulation is slightly larger, approaching 2000. These parameters as well as dye visualizations of the flow indicate that the vortex rings generated in these experiments primarily exhibit laminar flow behavior.[30] Accordingly, the interpolation of the DPIV data in later analyses does not introduce artifacts in the form of spurious flow features. To be sure, a comparison of measured velocity fields at the original spatial resolution (0.19×0.19 mm per pixel) and after enhancement via interpolation does not reveal any discernible differences in integrated flow parameters such as the instantaneous vortex ring circulation, or the location of critical points in the flow such as stagnation points.[30]

B. Free-swimming *Aurelia aurita* jellyfish

Jellyfish are unique among most animals in their heavy dependence on fluid transport for both locomotion and feeding. During locomotion, the animals use the surrounding ambient fluid to create vortex rings—one during the contractile power stroke and one during the relaxation recovery stroke.[14] The momentum imparted to the fluid in these vortices results in net thrust generation by the animals during locomotion. Similar vortical flows are also created by the animals to induce transport of prey and nutrients in the surrounding fluid toward the bell margin, where contact is made with the tentacles and oral appendages. This heavy dependence on fluid transport for behaviors that are critical to their survival suggests that useful design and optimization principles for effective transport[49,50] may be uncovered by studying the physical mechanisms whereby fluid transport is accomplished. The role of vortex ring dynamics is of particular interest in this regard. Quantitative measurements of the flow created by these animals enables a determination of whether lobe dynamics and vortex ring kinematics observed in previous theoretical and numerical models also exist in a naturally occurring biological flow that is much more unsteady.

Juvenile *Aurelia aurita* medusae (i.e., jellyfish with a characteristic bell-shaped body) were obtained from the Cabrillo Marine Aquarium (San Pedro, CA). The animals were transported on the day of quantitative visualization to a 75 gallon water tank at Caltech designed specifically to house jellyfish for DPIV measurements. A schematic of the facility is provided in Fig. 5.

A small background current was maintained in the tank to prohibit the tendency for jellyfish to swim toward walls and flow conditioners, where they are susceptible to damage. Seawater of appropriate salinity ($\approx$35 per mill), temperature ($\approx$15 °C), and filtrate size (less than 20 μm) was circulated by a small magnetic drive pump (Iwaki Co.). The temperature was regulated to ±1 °C by an inline electronic chiller (TWA Enterprises, Inc.). Organic waste created by the animals was treated by an inline canister filtration system (Nu-clear Filters). The walls of the tank were constructed from transparent acrylic to facilitate quantitative imaging experiments.

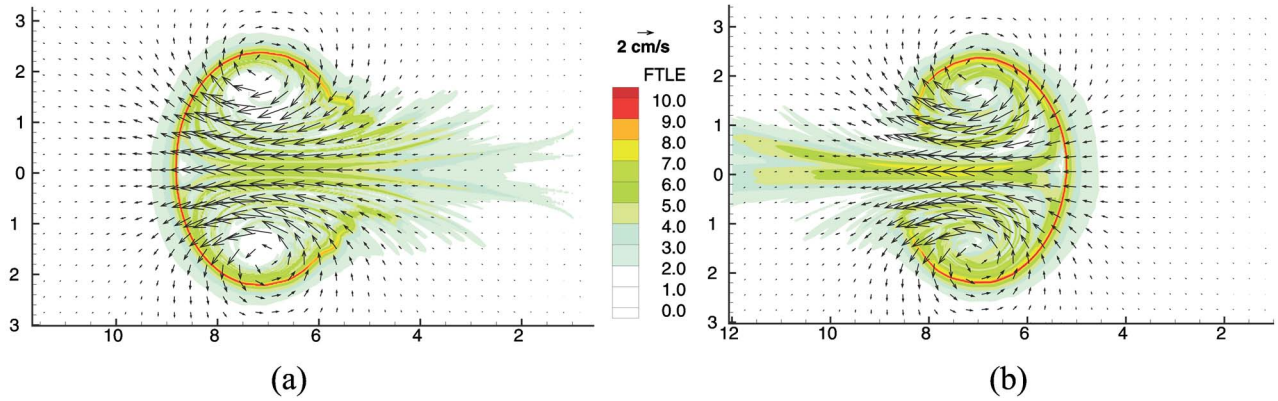

FIG. 6. (Color online) Contour plots of the FTLE fields computed from DPIV at time $t=3.4$ s, with an integration times $T=-3.4$ s and $T=3.4$ s in panels (a) and (b), respectively. Position coordinates are specified in centimeters.

Quantitative imaging was accomplished using DPIV. A laser sheet illuminated a two-dimensional plane of the flow inside the pseudokreisel. Incident light reflected by particles in the flow was captured by a CCD camera oriented so that its image plane was parallel to the laser sheet. Brine shrimp (used as feed) dispersed throughout the water tank provided a modest signal that could, in principle, be analyzed by DPIV. However, to increase the signal-to-noise ratio, additional 13 micron diameter (nominally) glass beads were seeded in the water tank. These particles increased the scattering of incident laser light, resulting in higher-quality images for interrogation.

Due to the lack of control of jellyfish motion within the tank, the laser system and camera were mounted on a three-axis traverse to facilitate movement of the measurement window, in accordance with the current location of the animal in the tank. This method increased the efficiency of the data collection process, since it was not necessary to wait for the animal to swim through a fixed measurement window. However, it is important to note that the camera and laser were kept in a fixed position during the process of image capture, to ensure that the flow fields were measured with respect to an inertial frame of reference. Velocity fields were computed using the same interrogation techniques implemented for the mechanically generated vortex rings described above.

IV. RESULTS

A. Mechanically generated vortex rings

1. LCS analysis

Figures 6(a) and 6(b) show color contour plots of the FTLE fields computed from the DPIV data at the arbitrary time $t=3.4$ s, with integration times of $T=-3.4$ s and $T=3.4$ s. Time $t=0$ corresponds to the initialization of vortex formation, i.e., the beginning of fluid ejection from the cylinder. The vortex is completely formed around $t=1$ s and propagates from right to left as time evolves. The FTLE fields were computed by the software package MANGEN, a dynamical systems computational toolset created by Francois Lekien of Princeton University. The algorithm can be summarized as follows:

At each time t, we have the following:

(1) A grid of particles $\mathbf{X}(t)$ is advected by the flow by numerically integrating the velocity field data with a fourth-order Runge-Kutta-Fehlberg algorithm to give $\mathbf{X}(t+T)$, which are the values of the flow map at each point. This numerical integration requires interpolating the velocity data, for which a third-order interpolator[51] was used.
(2) The spatial gradient of the flow map is obtain at each point in the initial grid by central differencing with neighboring grid points
(3) The FTLE is computed at each point in the initial grid by evaluating (1).

The previous three steps are repeated for a range of times t to provide a time series of FTLE fields.

A Cartesian grid was used for the FTLE computations shown in Fig. 6, with uniform spacing of 0.01 cm. The ridges of high FTLE values in each plot represent LCS. For Fig. 6(a), the LCS is an attracting LCS (aLCS) since $T<0$, and for Fig. 6(b) the LCS is a repelling LCS (rLCS) since $T>0$. The aLCS is analogous to the manifolds shown by the solid line in Fig. 3 and the rLCS represents the manifolds shown by the dashed lines in Fig. 3. The looping behavior of the manifolds shown in Fig. 3 is revealed in the FTLE fields of Fig. 6 if a longer integration time is chosen, as we will see (although it is already somewhat noticeable in the plots).

The time, $t=3.4$ s, at which we chose to show the FTLE field is somewhat arbitrary, and the integration length $|T|=3.4$ s is also somewhat arbitrary. For example, we could have chosen to show the FTLE fields at time $t=3.4$ s using integration times of $T=2$ and -2 s. If a smaller integration time is used, then not as much of the manifold is revealed, whereas if a longer integration time is used, more of the manifold is revealed. However supposing that the data begins at $t=0$, if we chose $T<-3.4$ s then we are restricted by the availability of data to show the FTLE field at some time $t>|T|$. Because the FTLE is a measure of the *linearized* growth rate about a trajectory, as $|T|$ becomes larger, the resolution of the FTLE computational grid typically must be increased. The integration length of $|T|=3.4$ s was chosen because it is long enough to reveal the boundary of the vor-

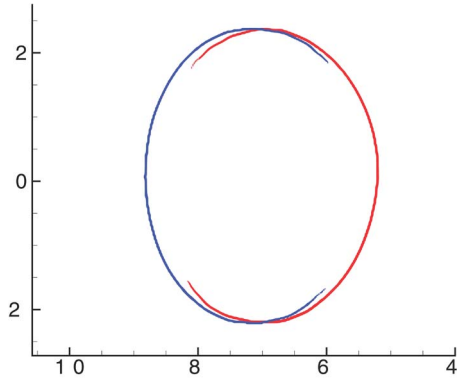

FIG. 7. (Color online) Intersection of aLCS (blue curve) and rLCS (red curve) define the vortex interior. Shown for $t=3.4$ s.

tex ring, yet short enough to keep the plot (and computation) from becoming overly complicated.

Superimposed on the FTLE contour plots of Fig. 6 is the DPIV velocity field data at $t=3.4$ s. Notice that it is impossible to define a vortex boundary from inspection of the velocity field. If we plot the two LCS given in Fig. 6(a) and 6(b) together, we obtain the plot given in Fig. 7. The LCS, up to their intersections, provide a well defined vortex boundary, as suggested by Shariff *et al.*[2,3] and Rom-Kedar *et al.*[10] These LCS can be thought of as material lines,[25] such that transport is locally tangent to these structures. They separate the circulating fluid that moves downstream with an average velocity equal to the speed of the vortex from the rest of the fluid. Because the LCS are time varying, it is the deformation and interaction of these coherent structures that allows fluid to be entrained or detrained; cf. Refs. 2, 3, and 11.

If the FTLE field shown in Fig. 6(b) is computed from a longer integration time T, we can obtain the LCS shown in Fig. 8, where we have zoomed in to the lower left hand corner of the vortex ring. The rLCS loops progressively back and forth. The intersection of this looping with the aLCS creates lobes. These empirical data are sufficient to validate previous theoretical and numerical predictions regarding the transport of fluid into and out of the interior of the vortex ring via the evolution of these lobes. The following analysis accomplishes this.

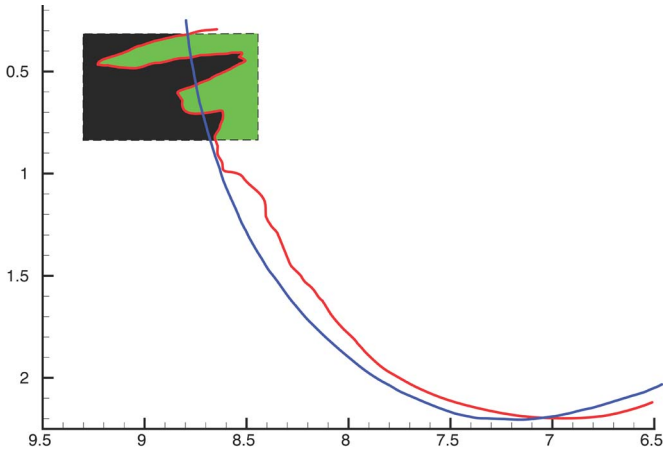

FIG. 8. (Color online) Looping of the rLCS. Superimposed is a rectangular parcel of fluid.

Suppose we place a rectangular parcel of fluid particles in the measured flow at time $t=3.4$ s and locate the parcel as shown by the dashed rectangle in Fig. 8. The vortex boundary is given by the aLCS (at least up to the intersection point of the two manifolds in the bottom right hand side of the plot; cf. Fig. 7). Thus the parcel of fluid intersects the interior and exterior of the vortex. Using the Eulerian velocity field description from DPIV, it would be impossible to determine specifically which particles are entrained, detrained, or remain inside or outside the vortex. However, we can make such a prediction from the LCS derived from the measured vortex ring flow. The particles in the rectangular parcel located "outside" the rLCS at time $t=3.4$ s are darkly colored, and those located inside the rLCS at that instant are lightly colored. The aforementioned theoretical and numerical results predict that as time evolves, all the lightly colored particles—even those outside the vortex ring at this instant—are entrained into the vortex interior, and all darkly colored particles—even those inside the vortex ring at this instant—will be left in the wake.

Figure 9 shows the time evolution of this parcel of fluid particles (as dictated by integrating the measured velocity field from DPIV) with the time evolution of the LCS. The LCS are shown by plotting the FTLE fields as in Fig. 6, but shading all level sets below some upper threshold white, and coloring the upper level sets for the forward and backward time FTLE fields. Figure 9(a) shows the initial location of the parcel, which is composed of 16110 particles, with 10250 darkly colored and 5860 lightly colored. The parcel initially becomes stretched into a thin filament as it is advected around the bottom of the vortex; cf. Fig. 9(b). As the parcel propagates up the other side of the vortex (which is itself moving relative to the laboratory frame), it forms lobes that are dictated by the looping of the aLCS. The looping of the aLCS is not shown in Fig. 9, but one can easily see its effect from the "spikes" formed by the parcel as it approaches the rear of the ring. As mentioned previously, the name attracting LCS implies that a parcel placed about this manifold will align with the manifold over time and analogously a parcel placed over the repelling LCS is stretched apart as time evolves. As the parcel continues to be advected by the flow, the lightly colored particles are entrained into the vortex while the darkly colored particles are detrained and left behind the vortex; Figs. 9(c) and 9(d). A movie of the evolution shown by the snapshots of Fig. 9 can be found at http://www.cds.caltech.edu/~marsden/research/demos/.

In Dabiri and Gharib[30] a variety of counterflow protocols were implemented to alter the vortex ring dynamics. These protocols were comprised of adding a constant counterflow initiated some time after vortex formation was initialized by the piston-cylinder apparatus. While these flows were more unsteady than the one analyzed above, LCS computed from data of these experiments all revealed lobe dynamics qualitatively similar to the no counterflow experiment analyzed here, thus demonstrating the robustness of these results.

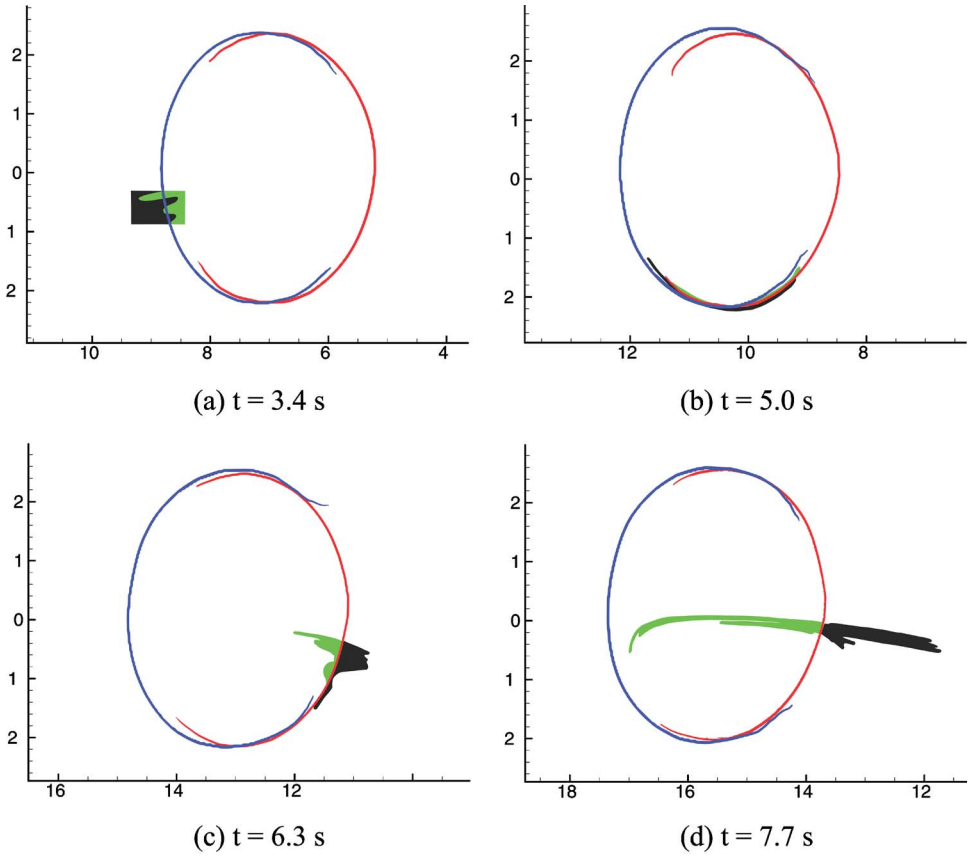

FIG. 9. (Color online) Evolution of lobes in empirical vortex rings.

In the works of Shariff *et al.*[1,2] and Rom-Kedar *et al.*,[11] the heteroclinic tangle geometry was obtained from vortex ring models and was revealed on Poincaré sections by exploiting the periodicity of the flow. In the simulations of the axisymmetric flow studied by Krasny and Nitsche,[12] a dominant frequency existed that was used to develop a Poincaré section, but it was clear that the unstable manifold evolved according to lower subharmonics, creating a more convoluted picture than the entanglement shown in Refs. 1, 2, and 11. However, the heteroclinic geometry for the flow considered here is based on empirical data and shows the *time-dependent geometry* of the entanglement without the need for Poincaré sections. This capability is important when periodicity is lacking, such as in the counterflow experiments discussed previously, or in the case of the swimming jellyfish studied later. Additionally, it is important to note that in aperiodic systems, the "stable and unstable manifolds" (more properly rLCS and aLCS) need not be infinite in length as in the periodic cases. Furthermore, it is not clear that lobe dynamics need exist in aperiodic flows in general. Along these lines, Joseph and Legras[47] studied the polar vortex using finite-size Lyapunov exponent fields to reveal LCS that demarcate a boundary of the vortex. Although the polar vortex has a monopole structure rather than the dipole configurations studied here (and other flow structures present) it was nevertheless shown that lobe dynamics were present, albeit much more faintly than for the flows considered here.

Although the mechanically generated rings are approximately axisymmetric, nonidealities in the experimental setup, such as reactive forces generated during the experiment or nonquiescent ambient fluid, lead to slight asymmetries in the azimuthal direction. These asymmetries manifest in the slight ordinate asymmetry of the FTLE fields; cf. Fig. 6. However, it is expected that swirl is negligible for the flow of the mechanically generated vortex rings, because swirl would only become noticeable farther downstream from the evolution studied here.[52] Therefore, it is justifiable to study the evolution of the LCS on two-dimensional sections, however, it is most desirable to understand the three-dimensional geometry of these structures. Such a three-dimensional geometry is *intuitively* some slightly deformed surface of revolution of the two-dimensional sections shown here, but knowing, for example, how lobe volume varies azimuthally, or how the intersections of the LCS vary azimuthally is important for understanding transport rates. The need for such a three-dimensional view becomes more compelling when the flow becomes more azimuthally asymmetric, such as in the case of the jellyfish; cf. Sec. IV B.

2. Comparison with Eulerian analysis

The use of instantaneous streamlines as an accurate representation of flow kinematics is valid strictly for steady flows. However, previous measurements of isolated vortex ring propagation[30] suggest the possibility of applying such methods to approximately describe quasisteady flow. In that case, the vortex boundary was determined by plotting streamlines of the measured flow in a reference frame propagating with the vortex ring. The cross-sectional area of the vortex ring was determined from an elliptical curve fit to the

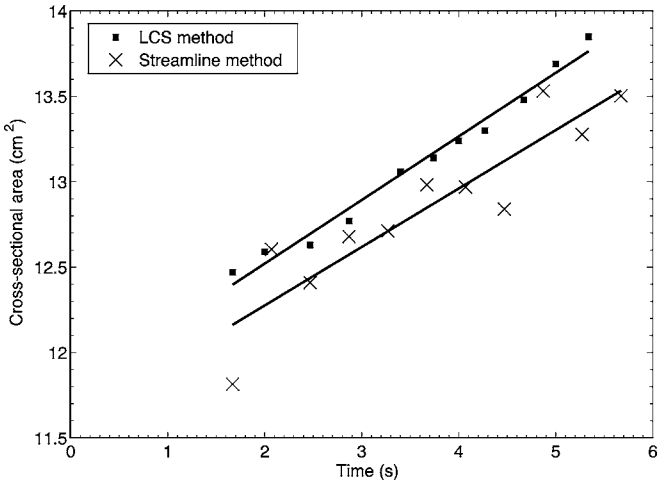

FIG. 10. Cross-sectional area of the vortex interior as a function of time as measured from the streamline method (Ref. 30) and the LCS method described in Sec. IV.

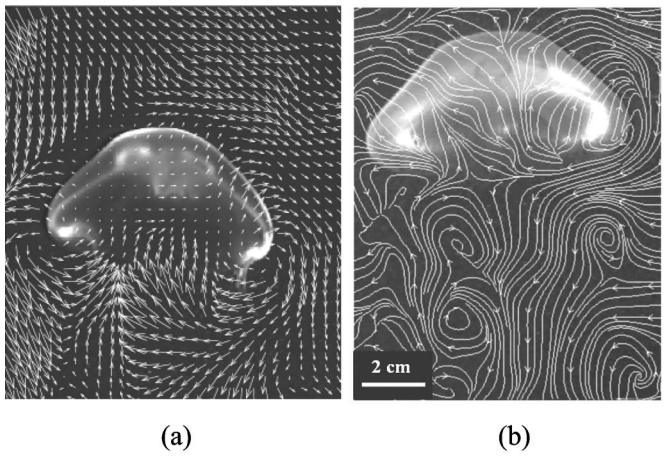

FIG. 11. Panel (a) shows DPIV measurements of the velocity field surrounding a free-swimming *Aurelia* jellyfish at an arbitrary time in its swimming motion. Panel (b) shows the instantaneous streamlines of the flow in the wake of a jellyfish similar to the one in panel (a).

(instantaneous) front and rear stagnation points of the vortex ring, as well as its radial extent. It is useful to compare the fidelity of the present LCS methods with quasisteady flow kinematics determined from such an Eulerian analysis.

Figure 10 plots the temporal trend in vortex ring cross-sectional area measured from the previous Eulerian analysis[30] along with data measured from the LCS method described above. The two trends are in close agreement, indicating the expected result that the Eulerian and Lagrangian analyses converge in the limit of steady flow. However, measurements from the LCS method tend to be less noisy. More importantly, the LCS method provides much more specific information regarding the transport of fluid (e.g., the results of the previous section, Sec. IV A 1) and it is not limited by flow unsteadiness as with the Eulerian perspective.

B. Free-swimming *Aurelia aurita* jellyfish

Figure 11 plots measurements of the velocity field and instantaneous streamlines generated by a free-swimming *Aurelia* jellyfish observed from the methods described in Sec. III B. The vortical wake behind the animal is visible and exhibits a flow geometry consistent with previous dye visualizations.[14] However, this Eulerian perspective provides no quantitative indication of the geometry of fluid transport, e.g., the magnitude or distribution of fluid transport between the animal and its surrounding, or the presence of lobe dynamics.

FTLE fields were computed from the DPIV data in a manner similar to what was described in Sec. IV A 1 for the mechanically generated rings. Figure 12(a) shows the FTLE field at a given instance in the neighborhood of the jellyfish.

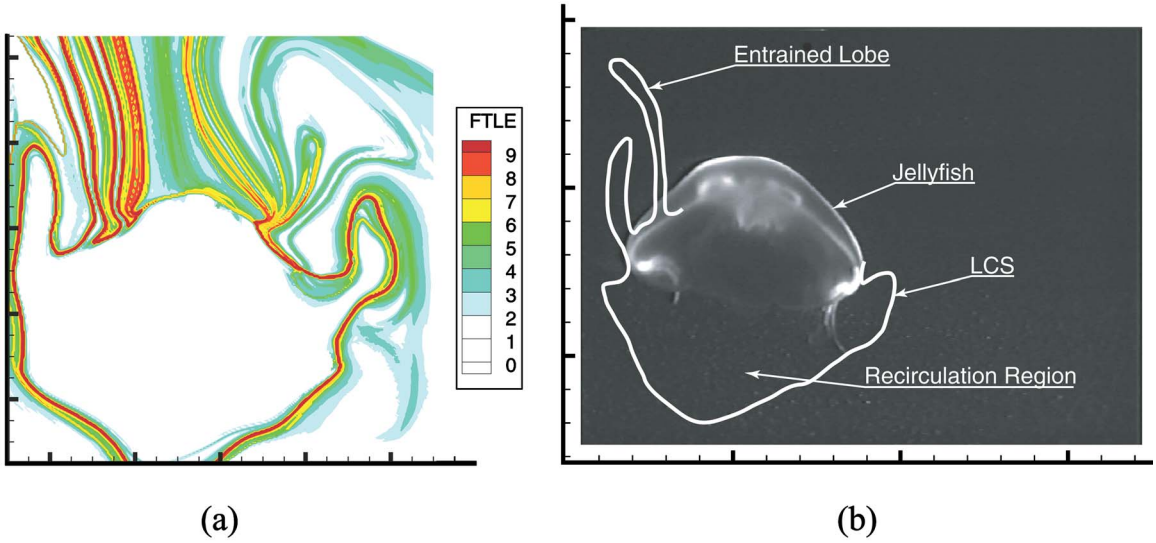

FIG. 12. (Color online) Panel (a) shows the FTLE field (T=13.3 s, grid spacing of 0.04 cm) at the same time as the measurement in Fig. 11(a). The FTLE field reveals an LCS, that is superimposed over the jellyfish at a slightly later time in panel (b). The evolution of the LCS indicates which regions of fluid are entrained and shows a recirculation zone behind the jellyfish.

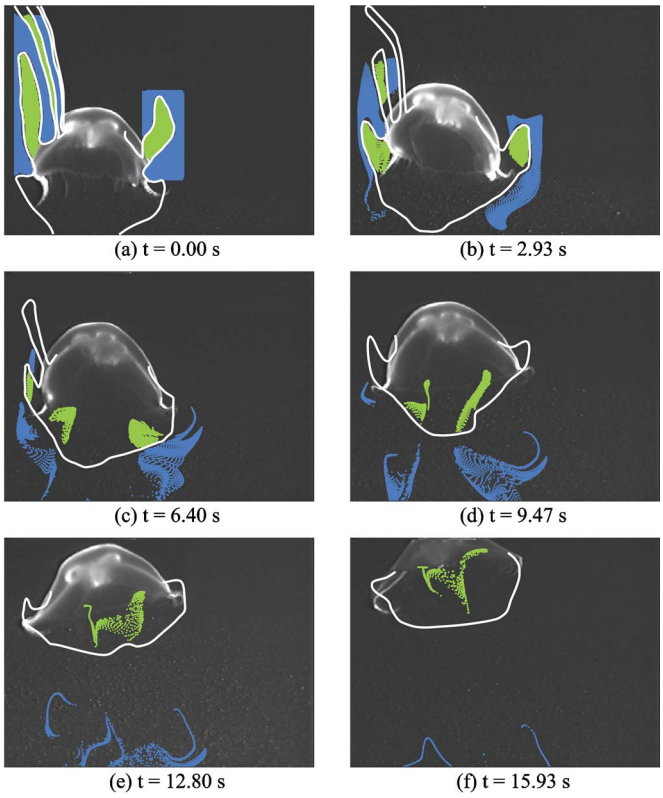

FIG. 13. (Color online) Evolution of lobes about jellyfish. The lobes distinguish which fluid is entrained into the subumbrellar region.

A very noticeable LCS exists in the FTLE field. Figure 12(b) plots the LCS (at a slightly later time) over the location of the jellyfish. In addition to discovering the existence of a closed region of the flow in contact with the sensory apparatus of the animal (in the subumbrellar region), the LCS also reveals the presence of lobe dynamics. An analysis similar to that in Fig. 9 demonstrates that the lobes formed at the upstream end of the animal dictate which portions of the ambient fluid are sampled by the animal (via passive filter feeding and prey capture) and which portions pass by the animal without interacting, as shown in Fig. 13. A movie of the evolution shown by the snapshots of Fig. 13 can be found at http://www.cds.caltech.edu/~marsden/research/demos/. The computations presented here were repeated on a second set of data collected from a similar jellyfish experiment, resulting in similar lobe dynamics. It is important to keep in mind that the LCS shown here are cross sections of two-dimensional surfaces that exist for the fully three-dimensional flow. Progress is currently being made on obtaining the full three-dimensional lobe dynamic geometry.

V. CONCLUSIONS

In this paper we have shown, using DPIV data for the velocity fields of both mechanically generated vortices and the flow around a free-swimming *Aurelia aurita* jellyfish, that heteroclinic and lobe-like structures are present for fully unsteady flows. For the mechanically generated vortex rings, a computational study using Lagrangian coherent structures (LCS) revealed lobe dynamics that were consistent with previous analytic and numeric studies, but were able to do so without the need for a perturbative assumption or periodicity or the use of Poincaré sections. Remarkably, a similar analysis applied to the measured flow about the jellyfish demonstrated qualitatively similar lobe dynamics. The lobes reveal the mechanism for entrainment in the jellyfish flow, which is critical to its feeding.

The results presented in this paper are noteworthy, not only for their important biological implications (which are beyond the scope of the present paper), but more immediately for their ability to reveal governing fluid transport mechanisms in empirical, unsteady flows. It is reasonable to suggest that other complex flows of interest in nature and technology should be examined within the framework described here to uncover key fluid transport concepts such as lobe dynamics. In particular, flows in the cardiovascular system and microfluidics represent significant opportunities for such an analysis.

The results of the present paper demonstrate that, in comparison with a Lagrangian analysis, much of these fluid dynamical features are missed in a traditional Eulerian analyses based on velocity field snapshots or on instantaneous streamlines. Other Lagrangian studies have primarily focused on periodic or nearly periodic model flows for both theoretical and numerical investigations. Advantages of the LCS methods used in this paper are their applicability to fully unsteady flows, and the relative ease of implementation. In addition, the extensions of the experimental methods to obtain velocity data, the LCS theory, and the MANGEN software to handle fully three-dimensional flows is currently underway (see also Ref. 53), which will make the analyses even more interesting.

Although lobe dynamics are ubiquitous for periodically perturbed two-dimensional incompressible fluid flows (which are Hamiltonian systems) and for certain 3D flows as well, it is not obvious that similar geometries should occur in naturally occurring aperiodic flows. There has been a need to better understand both the conditions under which such structures arise in vortex flows of practical importance to engineering and biology, and which theoretical and computational tools can be applied or extended to study fluid transport as well as other relevant topics, such as multiobjective optimization, in such systems. In this paper we have provided some important steps toward such interesting goals.

ACKNOWLEDGMENTS

The authors are very grateful to Francois Lekien of Princeton University for the use of the software MANGEN. We would also like to thank Vered Rom-Kedar of the Weizmann Institute of Science for her insightful comments and valuable suggestions. This paper was partially supported by ONR-MURI Contract No. 00000916.

[1] K. Shariff and A. Leonard, "Vortex rings," Annu. Rev. Fluid Mech. **24**, 235 (1992).
[2] K. Shariff, "Dynamics of a class of vortex rings," Ph.D. thesis, Stanford University, 1989.
[3] K. Shariff, A. Leonard, and J. H. Ferziger, "Dynamics of a class of vortex rings," NASA Technical Memorandum 102257, 1989.
[4] A. Leonard, V. Rom-Kedar, and S. Wiggins, "Fluid mixing and dynamical

systems," *Proceedings of the International Conference on The Physics of Chaos and Systems Far from Equilibrium*, Nucl. Phys. B, Proc. Suppl. **2**, 179 (1987).
[5]D. W. Moore, "The velocity of a vortex ring with a thin core of elliptical cross-section," Proc. R. Soc. London, Ser. A **370**, 407 (1980).
[6]H. Yamada and T. Matsui, "Preliminary-study of mutual slip-through of a pair of vortices," Phys. Fluids **21**, 292 (1978).
[7]B. Sturtevant, L. Hesselink, and J. F. Haas, "Interaction of weak shock-waves with random media," J. Acoust. Soc. Am. **65**, S96 (1979).
[8]H. K. Moffatt and D. W. Moore, "The response of Hill's vortex to a small axisymmetric disturbance," J. Fluid Mech. **87**, 749 (1978).
[9]C. Pozrikidis, "The nonlinear instability of Hill's vortex," J. Fluid Mech. **168**, 337 (1986).
[10]V. Rom-Kedar and S. Wiggins, "Transport in two-dimensional maps," Arch. Ration. Mech. Anal. **109**, 239 (1990).
[11]V. Rom-Kedar, A. Leonard, and S. Wiggins, "An analytical study of transport, mixing and chaos in an unsteady vortical flow," J. Fluid Mech. **214**, 347 (1990).
[12]R. Krasny and M. Nitsche, "The onset of chaos in vortex sheet flow," J. Fluid Mech. **454**, 47 (2002).
[13]G. F. Carnevale and R. C. Kloosterziel, "Lobe shedding from propagating vortices," Physica D **76**, 147 (1994).
[14]J. O. Dabiri, S. P. Colin, J. H. Costello, and M. Gharib, "Flow patterns generated by oblated medusan jellyfish: Field measurements and laboratory analyses," J. Exp. Biol. **208**, 1257 (2005).
[15]R. J. Adrian, "Particle-imaging techniques for experimental fluid-mechanics," Annu. Rev. Fluid Mech. **23**, 261 (1991).
[16]C. E. Willert and M. Gharib, "Digital particle image velocimetry," Exp. Fluids **10**, 181 (1991).
[17]J. R. Hove, R. W. Koster, A. S. Forouhar, G. Acevedo-Bolton, S. E. Fraser, and M. Gharib, "Intracardiac fluid forces are an essential epigenetic factor for embryonic cardiogenesis," Nature **421**, 172 (2003).
[18]H. A. Stone, A. D. Stroock, and A. Ajdari, "Engineering flows in small devices: microfluidics toward a lab-on-a-chip," Annu. Rev. Fluid Mech. **36**, 381 (2004).
[19]F. Bottausci, I. Mezić, C. D. Meinhart, and C. Cardonne, "Mixing in the shear superposition micromixer: Three-dimensional analysis," Philos. Trans. R. Soc. London, Ser. A **362**, 1001 (2004).
[20]C. A. Taylor and M. T. Draney, "Experimental and computational methods in cardiovascular fluid mechanics," Annu. Rev. Fluid Mech. **36**, 197 (2004).
[21]G. Haller and G. Yuan, "Lagrangian coherent structures and mixing in two-dimensional turbulence," Physica D **147**, 352 (2000).
[22]G. Haller, "Distinguished material surfaces and coherent structures in 3-dimensional fluid flows," Physica D **149**, 248 (2001).
[23]G. Haller, "Lagrangian structures and the rate of strain in a partition of two-dimensional turbulence," Phys. Fluids **13**, 3365 (2001).
[24]G. Haller, "Lagrangian coherent structures from approximate velocity data," Phys. Fluids **14**, 1851 (2002).
[25]S. C. Shadden, F. Lekien, and J. E. Marsden, "Definition and properties of Lagrangian coherent structures from finite-time Lyapunov exponents in two-dimensional aperiodic flows," Physica D **212**, 271 (2005).
[26]F. Sotiropoulos, D. R. Webster, and T. C. Lackey, "Experiments on Lagrangian transport in steady vortex-breakdown bubbles in a confined swirling flow," J. Fluid Mech. **466**, 215 (2002).
[27]G. A. Voth, G. Haller, and J. P. Gollub, "Experimental measurements of stretching fields in fluid mixing," Phys. Rev. Lett. **88**, 254501 (2002).
[28]P. E. Arratia, G. A. Voth, and J. P. Gollub, "Stretching and mixing of non-Newtonian fluids in time-periodic flows," Phys. Fluids **17**, 053102 (2005).
[29]P. G. Saffman, "Dynamics of vorticity," J. Fluid Mech. **106**, 49 (1981).
[30]J. O. Dabiri and M. Gharib, "Fluid entrainment by isolated vortex rings," J. Fluid Mech. **511**, 311 (2004).
[31]H. Lamb, *Hydrodynamics* (Cambridge University Press, Cambridge, 1932).
[32]J. Guckenheimer and P. Holmes, *Nonlinear Oscillations, Dynamical Systems and Bifurcations of Vector Fields* (Springer-Verlag, New York, 1983).
[33]V. K. Melnikov, "On the stability of the center for time periodic perturbations," Trans. Mosc. Math. Soc. **12**, 1 (1963).
[34]J. O. Dabiri and M. Gharib, "Starting flow through nozzles with temporally variable exit diameter," J. Fluid Mech. **538**, 111 (2005).
[35]J. Norbury, "A family of steady vortex rings," J. Fluid Mech. **51**, 417 (1973).
[36]J. M. Ottino, *The Kinematics of Mixing: Stretching, Chaos, and Transport* (Cambridge University Press, Cambridge, 1989).
[37]G. Haller and A. C. Poje, "Finite time transport in aperiodic flows," Physica D **119**, 352 (1998).
[38]G. Haller, "Finding finite-time invariant manifolds in two-dimensional velocity fields," Chaos **10**, 99 (2000).
[39]S. Wiggins, "The dynamical systems approach to Langrangian transport in oceanic flows," Annu. Rev. Fluid Mech. **37**, 295 (2005).
[40]C. K. R. T. Jones and S. Winkler, "Invariant manifolds and Lagrangian dynamics in the ocean and atmosphere," *Handbook of Dynamical Systems: Towards Applications*, edited by B. Fiedler (Elsevier, Amsterdam, 2002), p. 55.
[41]C. Coulliette and S. Wiggins, "Intergyre transport in a wind-driven, quasi-geostrophic double gyre: An application of lobe dynamics," Nonlinear Processes Geophys. **7**, 59 (2000).
[42]H. E. Deese, L. J. Pratt, and K. R. Helfrich, "A laboratory model of exchange and mixing between western boundary layers and sub-basin recirculation gyres," J. Phys. Oceanogr. **32**, 1870 (2002).
[43]R. T. Pierrehumbert, "Large-scale horizontal mixing in planetary atmospheres," Phys. Fluids A **3**, 1250 (1991).
[44]R. T. Pierrehumbert and H. Yang, "Global chaotic mixing on isentropic surfaces," J. Atmos. Sci. **50**, 2462 (1993).
[45]G. Haller, "An objective definition of a vortex," J. Fluid Mech. **525**, 1 (2005).
[46]F. Lekien, C. Coulliette, A. J. Mariano, E. H. Ryan, L. K. Shay, G. Haller, and J. E. Marsden, "Pollution release tied to invariant manifolds: A case study for the coast of Florida," Physica D **210**, 1 (2005).
[47]B. Joseph and B. Legras, "Relation between kinematic boundaries, stirring, and barriers for the Antartic polar vortex," J. Atmos. Sci. **59**, 1198 (2002).
[48]M. Gharib, E. Rambod, and K. Shariff, "A universal time scale for vortex ring formation," J. Fluid Mech. **360**, 121 (1998).
[49]J. O. Dabiri and M. Gharib, "The role of optimal vortex formation in biological fluid transport," Proc. R. Soc. London, Ser. B **272**, 1557 (2005).
[50]P. S. Krueger and M. Gharib, "Thrust augmentation and vortex ring evolution in a fully pulsed jet," AIAA J. **43**, 792 (2005).
[51]F. Lekien and J. Marsden, "Tricubic interpolation in three dimensions," Int. J. Numer. Methods Eng. **63**, 455 (2005).
[52]J. O. Dabiri and M. Gharib, "Starting flow through nozzles with temporally variable exit diameter," J. Fluid Mech. **538**, 111 (2005).
[53]K. Padberg, "Numerical analysis of chaotic transport in dynamical systems," Ph.D. thesis, University of Paderborn, 2005.